applied sciences

MDPI

Article

Thermal Computational Fluid Dynamics Simulation of Two Designs of Direct Dehydrators for Agricultural Products

Said Arturo Rodríguez-Romero [1], Manuel Toledano-Ayala [2], Gonzalo Macías-Bobadilla [2], Edgar Alejandro Rivas-Araiza [2], Priscila Sarai Flores-Aguilar [1] and Genaro Martín Soto-Zarazúa [1,*]

[1] Facultad de Ingenieria Campus Amazcala, Universidad Autonoma de Queretaro, El Marques 76265, Mexico; srodriguez72@alumnos.uaq.mx (S.A.R.-R.)
[2] Facultad de Ingenieria, Universidad Autonoma de Queretaro, Cerro de las Campanas, Queretaro 76010, Mexico
* Correspondence: soto_zarazua@yahoo.com.mx

Abstract: The dehydration process modifies the physical and chemical characteristics of certain crops, thereby increasing their shelf life and consequently reducing the organic waste generated. This process is contingent upon maintaining optimal temperature and humidity levels to prevent deterioration of the product. As indirect dehydrators have a high energy demand, new designs are required that facilitate the uniform distribution of air with a high-volume capacity of 100 kg per day. In the present study, computational fluid dynamics (CFD) techniques were employed to assess the drying performance of two dehydrator models. The simulations were executed in Solidworks 2020 and Flow Simulation, and they examined temperature distribution and velocity within the interior of the dehydrators. In Model 1, an inlet volume flow of 0.08 m^3 s^{-1} and a heat source of 3.5 kW are considered, within a volume of 2.11 m^3. In Model 2, an inlet volume flow of 0.03 m^3 s^{-1} and two heat source of 2.5 kW are considered, within a volume of 2.02 m^3. Model 1 was unable to achieve uniform air distribution within the drying chamber. In contrast, Model 2 demonstrated uniform velocity and temperature across the majority of the drying chamber, making it a superior option.

Keywords: dehydrator; direct dryer; mechanical design; computational fluid dynamics; Solidworks; simulation; agriculture

check for updates

Citation: Rodríguez-Romero, S.A.; Toledano-Ayala, M.; Macías-Bobadilla, G.; Rivas-Araiza, E.A.; Flores-Aguilar, P.S.; Soto-Zarazúa, G.M. Thermal Computational Fluid Dynamics Simulation of Two Designs of Direct Dehydrators for Agricultural Products. *Appl. Sci.* **2024**, *14*, 8472. https://doi.org/10.3390/app14188472

Academic Editor: Cesare Biserni

Received: 2 August 2024
Revised: 3 September 2024
Accepted: 14 September 2024
Published: 20 September 2024

Copyright: © 2024 by the authors. Licensee MDPI, Basel, Switzerland. This article is an open access article distributed under the terms and conditions of the Creative Commons Attribution (CC BY) license (https://creativecommons.org/licenses/by/4.0/).

1. Introduction

The dehydration of food is one of the oldest and most effective techniques for preserving food, extending its shelf life without the need for artificial preservatives [1]. By reducing the weight and volume of food, dehydration also facilitates storage and transportation, lowering costs and the environmental impact associated with the distribution of fresh food [2–4]. Additionally, by utilizing renewable energy sources, such as solar power, for the dehydration process, the ecological footprint can be further minimized [5,6]. This practice not only contributes to food security and waste reduction but also supports the local economy by allowing producers to preserve surplus harvests and sell them out of season [7].

Drying equipment is categorized as a direct or adiabatic dryer. In the first category, the product to be dried is directly exposed to hot air, and in the second category, indirect or non-adiabatic dryers, heat is transferred from a medium in contact with the product. Among direct dryers, tray dryers are the form most commonly used for small-scale production, due to their simple construction and instrumentation [8,9]. One advantage of this type of equipment is their uniformity in drying products, which is achieved through temperature-controlled environments. Fuzzy logic (FL) has been employed successfully in the control of temperature and air flow in non-linear systems, demonstrating a greater efficacy than proportional–integral (PI) controllers. This approach has demonstrated the capacity to reduce energy and time demands, as well as the ability to adapt and operate under a wide

range of conditions while maintaining product quality. This ensures the economic viability of the equipment [5,10–12]. The main disadvantages of direct dehydrators are the lengthy drying time of approximately 50 h per load and their high energy consumption, which accounts for about 25% of the total energy consumed by the agribusiness industry. Although the traditional drying process relies solely on solar radiation, it results in a markedly slow drying time, often taking up to three days, depending on environmental conditions. Additionally, several external factors, such as animals, dust, and microorganisms, can potentially contaminate the product. This justifies the use of dehydrators, which accelerate the drying process and minimize the risk of contamination [13–15].

The temperature range for drying agricultural products varies depending on the specific product in question. However, the most limiting factor is the drying air, which must be hot and low in humidity. The temperature range for dryer operation has been found to vary from 40 °C to 70 °C, depending on the product. The current improvements in dehydrators include the implementation of an efficient design to ensure the proper drying conditions and hybrid or solar systems that aim to replace the use of fossil energy [4,7,15–18]. However, the industrial type of dehydrators are still mostly electric and the experimental hybrid ones are smaller than the design proposed in this research.

In recent decades, significant research has been conducted seeking to elucidate the chemical and physical alterations in the drying process and to develop innovative techniques in order to avert unfavorable quality deterioration. The application of computational fluid dynamics (CFD) in the dehydration process enhances the efficiency and uniformity of drying by accurately simulating and optimizing airflow and heat transfer within dehydrators [19,20]. Additionally, CFD is a valuable software tool used for predicting the performance and characteristics of air movement. It provides a solution to engineering challenges, improves process control, and reduces resource expenditures, including energy, time, and costs [21–25]. Furthermore, modern computers have sufficient processing power to enable the implementation of this method, making it accessible and affordable [26,27]. Although the simulation information can describe the entire fluid, experimental information is necessary to assess accuracy and reliability in computational simulations and to confirm its performance [28].

In the pursuit of optimizing agricultural practices, efficient food dehydration processes play a crucial role in preserving crop quality and extending shelf life. CFD methods were utilized to analyze and compare the air temperature, airflow direction, and velocity in two distinct dehydrator designs. The aim of this research was to design and simulate an efficient and high-capacity dehydrator that optimizes drying process and minimizes energy usage.

2. Materials and Methods

The work was conducted at the Universidad Autónoma de Querétaro, Amazcala campus, located in Amazcala, El Marqués, Querétaro. In this study, the methodology proposed by Shigley in 2011 [25] was employed for the design of two direct tray dehydrators, each with a capacity of 100 kg per load. SolidWorks Premium 2020 SP1.0 software was utilized to create and assemble the 3D CAD components that constitute the design of the dehydrators (Figures 1–4). The Flow Simulation tool was used to evaluate the air performance relative to temperature, distribution, and velocity in the models.

Flow Simulation solves the Navier–Stokes equations, which describe the laws of mass, momentum, and energy conservation (Equations (1)–(3)):

$$\frac{\partial \rho}{\partial t} + \frac{\partial}{\partial x_i}(\rho u_i) = S_M^p, \tag{1}$$

$$\frac{\partial \rho u_i}{\partial t} + \frac{\partial}{\partial x_j}(\rho u_i u_j) + \frac{\partial p}{\partial x_i} = \frac{\partial}{\partial x_j}\left(\tau_{ij} + \tau_{ij}^R\right) + S_i + S_{Ii}^p,\ i = 1,2,3;\ j = 1,2,3 \tag{2}$$

$$\frac{\partial \rho H}{\partial t} + \frac{\partial \rho u_i H}{\partial x_i} = \frac{\partial}{\partial x_i}\left(u_j\left(\tau_{ij} + \tau_{ij}^R\right) + q_i\right) + \frac{\partial p}{\partial t} - \tau_{ij}^R \frac{\partial u_i}{\partial x_j} + \rho\varepsilon + + S_i u_i + S_H^p + Q_H$$

$$H = h + \frac{u^2}{2} + \frac{5}{3}k - \frac{\Omega^2 r^2}{2} - \sum_m h_m^0 y_m \quad (3)$$

where u is the fluid velocity, ρ is the fluid density, S_i is a mass-distributed external force per unit mass due to a porous media resistance $\left(S_i^{porous}\right)$, a gravity ($S_i^{gravity} = \rho g_i$, where g_i is the gravitational acceleration component along the i-th coordinate direction), and the coordinate system's rotation $\left(S_i^{rotation}\right)$; i.e., $S_i = S_i^{porous} + S_i^{gravity} + S_i^{rotation}$, h is the thermal enthalpy; S_M^p, S_{Ii}^p, S_H^p are additional interfacial exchange terms due to Euler–Lagrange particle interaction; Q_H is a heat source per unit volume, τ_{ij} is the viscous shear-stress tensor, q_i is the diffusive heat flux, Ω is the angular velocity of the rotating coordinate system, r is the distance from a point to the rotation-reference frame, k is the kinetic energy of turbulence, h_m^0 is an individual thermal enthalpy of the m-th mixture component, y_m is a concentration of the m-th mixture component. The subscripts are used to denote summation over the three coordinate directions [29]. The Flow Simulation tool allows researchers to predict simultaneous heat transfer in solids and fluids with energy exchange, as described in Equation (4):

$$\frac{\partial \rho e}{\partial t} = \frac{\partial}{\partial x_i}\left(\lambda_i \frac{\partial T}{\partial x_i}\right) + Q_H \quad (4)$$

where e is the specific internal energy, $e = C \cdot T$, C is specific heat, Q_H is specific heat release per unit volume, and λ_i are the eigenvalues of the thermal conductivity tensor [29].

Model 1 is displayed in Figure 1, immediately below.

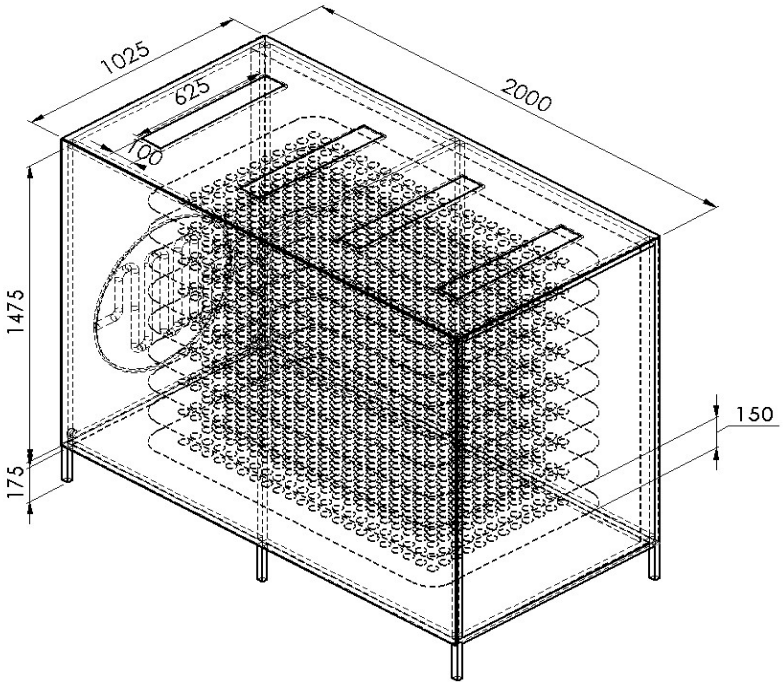


Figure 1. A 3D isometric view of the Model 1 dehydrator.

The geometry of dehydrator Model 1, with all measurements indicated in millimeters, is displayed above (Figure 1). Given that the equipment will be in contact with food products, AISI 304 stainless steel was selected as the material in order to ensure product safety and quality. This specific material has a thermal conductivity of 16 W m^{-2} K^{-1} and a density of 8 g m^{-3}. The equipment's mass was calculated by the software to be 926.2 kg, and the model's volume was determined to be 2.11 m^3.

The Flow Simulation tool was employed to simulate the inlet of air to aid in an analysis of internal functions. The boundary conditions are illustrated in Figure 2, and comprise a heat source of 3.5 kW, a volumetric flow of 0.08 m^3s^{-1} at 30 °C, and an environmental pressure of 101.3 MPa. Three primary objectives were established to ensure that the program would reach a convergence point and that the required computational time for the simulation would remain within acceptable limits: the fluid average temperature, the average total temperature of the equipment, and the solid average temperature were the specific parameters targeted. Furthermore, the software was configured to utilize automatic iterations, which identified the optimal solution through 168 iterations. This process excluded scenarios in which the temperature reached the point of melting the material and instances of a vortex forming within the interior of the equipment due to pressure imbalances between the inlet air and the surrounding environment. A global mesh was automatically constructed; Level 3 was selected for analysis due to the equipment's size and to reduce the computational time required for each simulation. Additionally, air velocity, direction, and temperature plots were incorporated into the model, along with a plot of the tray surface temperature. These were included in order to illustrate the heat transfer performance of the solid.

The second version of the equipment was designed based on the identification of shortcomings in the air distribution for Model 1. Again, AISI 304 stainless steel was selected as the material, exhibiting the aforementioned properties. Figure 3 illustrates the geometric configuration of the second dehydrator, with all measurements expressed in millimeters. In this instance, the volume calculated by the program was 2.02 m^3, with a mass of 395.5 kg.

Model 2 is described in Figure 3, following the subsequent figure.

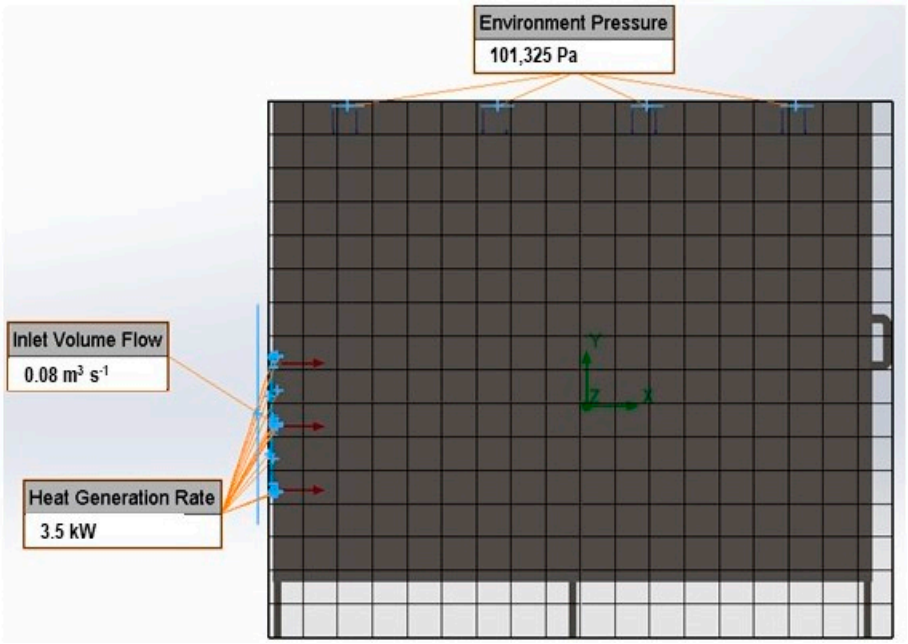


Figure 2. Lateral view of boundary conditions and mesh diagram of the Model 1 dehydrator.

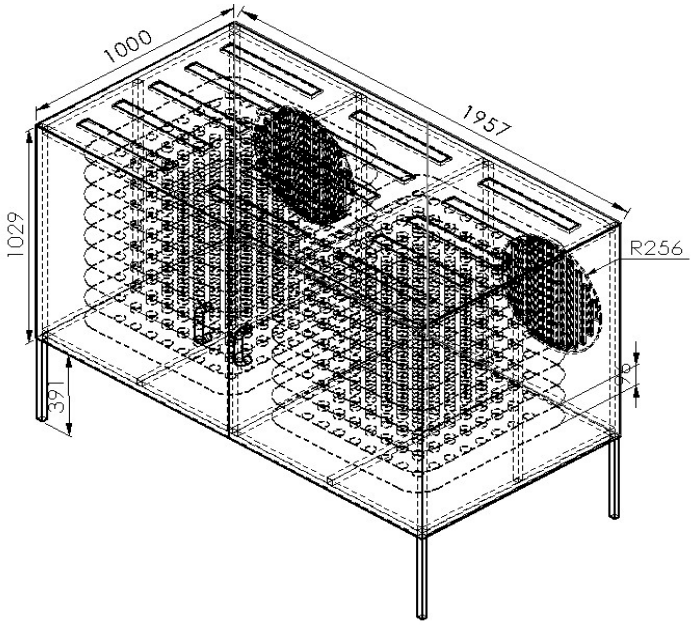


Figure 3. A 3D isometric view of the Model 2 dehydrator.

The Flow Simulation tool was once more employed to simulate the air performance in the enhanced design, with the analysis being conducted internally. The boundary conditions are detailed in Figure 4, and consist of two 1.5 kW heat sources, a volumetric flow of 0.02 m^3s^{-1} at 30 °C, and an environmental pressure of 101.3 MPa. To achieve the desired convergence of the solver, the previously outlined objectives must be met, namely, the fluid average temperature, the average total temperature of the equipment, and the solid average temperature. Furthermore, a configuration with automatic iterations was utilized, in which 224 of such iterations were employed to solve the model, with the exception of those instances where the material was melted and those instances where a vortex formed within the dehydrator. The global meshing Level 3 was selected, and the same plots mentioned before were included in the model for comparison of the air performance of the two pieces of equipment.

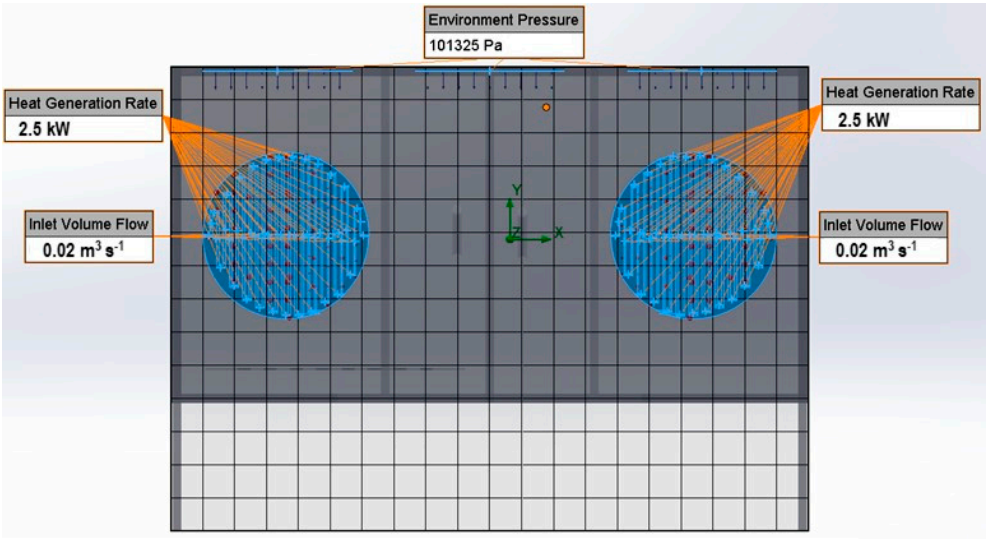


Figure 4. Frontal view of boundary conditions and mesh diagram of the Model 2 dehydrator.

All simulations were conducted on a Huawei MateBook 14 laptop, equipped with an AMD Ryzen 7 4800H processor with Radeon Graphics, operating at 2.90 GHz, and with 8 GB of RAM.

3. Results

Comparative studies on tray dehydrators indicate that an optimal airflow range is between 0.003 and 0.18 m^3s^{-1}. However, the key distinction between our designs and the existing models is the significantly enlarged drying chamber volume, which is approximately 10 times larger than the typical capacity of other reported devices [23,30,31]. The results obtained with the flow simulation tool are presented in Figure 5. In order to achieve a uniform air distribution throughout the drying chamber, a flow rate of 0.08 m^3s^{-1} was selected, which is within the previously mentioned range. This value was obtained following the completion of several simulations, during which it was determined that a lower flow rate would not result in the uniform distribution of air within the drying chamber, while a higher flow rate would prevent the heating of the air to a temperature exceeding 40 °C.

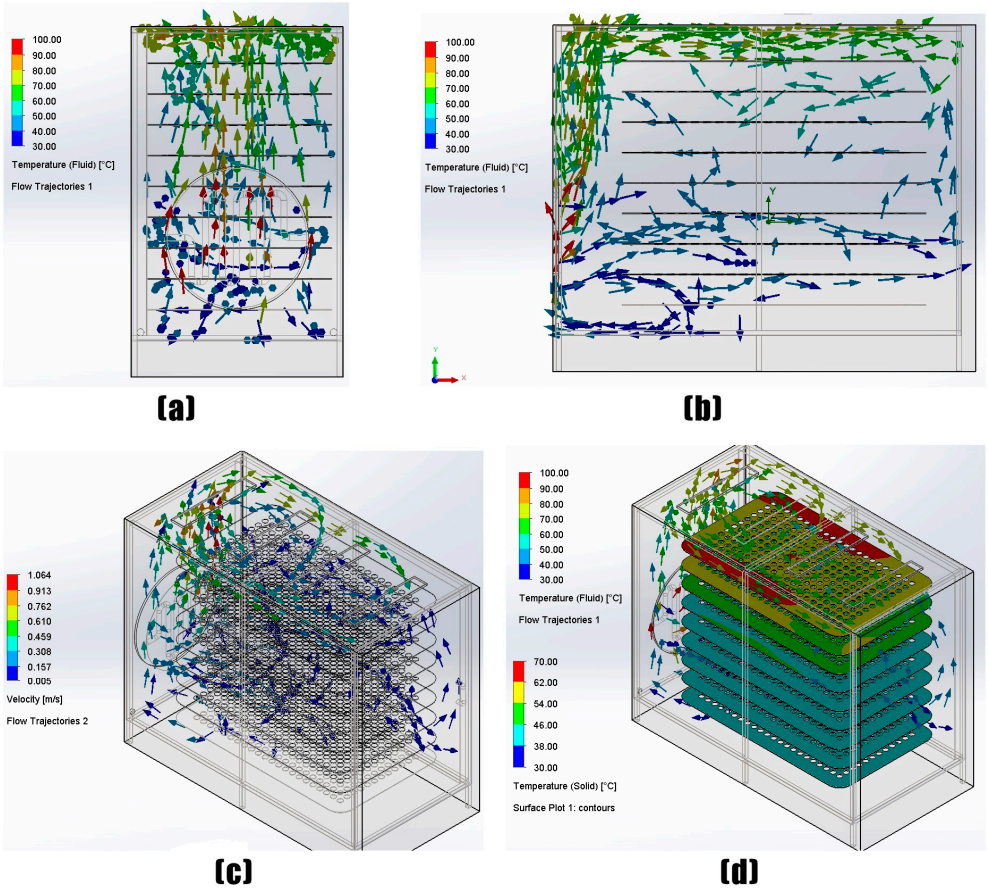


Figure 5. Different views of the Model 1 dehydrator air temperature, including tray temperatures: (**a**) frontal, (**b**) lateral, (**c**) isometric, and (**d**) isometric.

The temperature at the bottom of the equipment remains at 30 °C, while the temperature at the top reaches 70–80 °C. The inlet air, where the heat source is located, is the hottest part, reaching more than 100 °C. This causes an issue of temperature distribution, as there is no uniformity in the temperatures of the dry food, which is not optimal. Furthermore, the temperatures of the trays vary, demonstrating a potential impact on biological products. In the initial six trays, the temperature remains within the optimal range of 38 to 42 °C, indicating satisfactory thermal conditions. The seventh tray reaches temperatures between 46 and 54 °C, while the last two trays have temperatures between 46 and 70 °C, which are

problematic for agricultural products. The minimum air velocity in the drying chamber is 0.005 m s^{-1}, while the maximum is 1.06 m s^{-1}. It can be observed that within the majority of the area of the chamber, the velocity is between 0.005 and 0.3 m s^{-1}, ensuring that a vortex will not be formed. This model is unsuitable for a drying process. In order to improve the efficiency of the air distribution process, it is necessary to modify the position of the fan and the configuration of the equipment (Figure 5).

The issues identified in the initial model were taken into consideration during the development of the new dehydrator. This time, a horizontal geometry was selected, and two fans were positioned to ensure optimal air distribution. Figure 6 illustrates the results of the flow simulation. It can be observed that the air distribution in this case is superior to that of the previous model. The slower flow rate of 0.03 m^3s^{-1} ensures the heating of more air to the optimal range. Also, the isometric view reveals the presence of vortices in the corners of the equipment, a condition which must be modified.

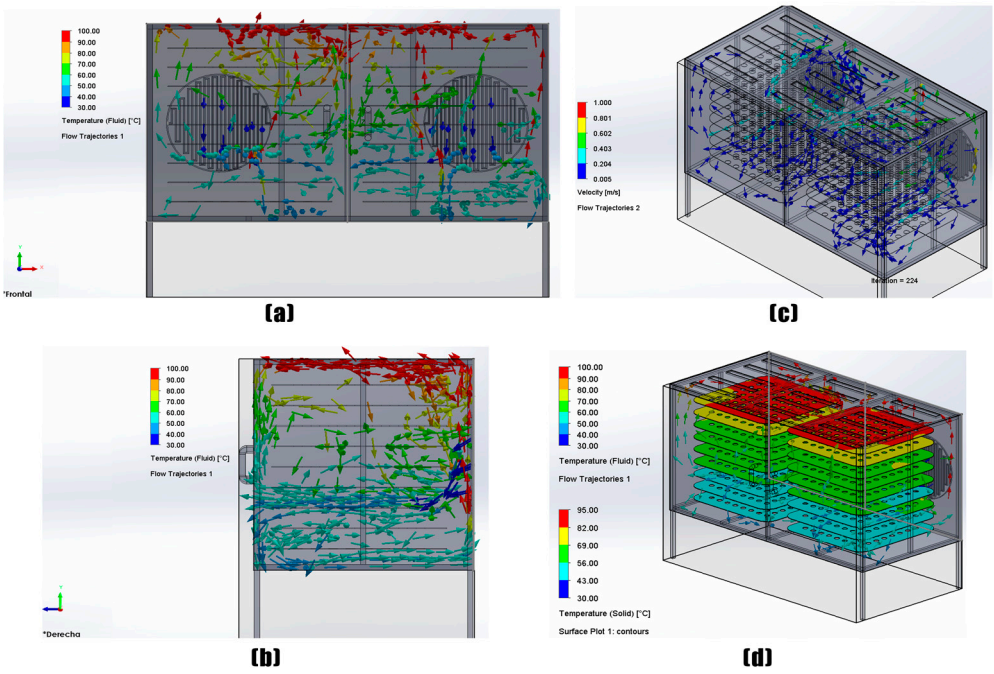


Figure 6. Different views of the Model 2 dehydrator air temperature and velocity, including tray temperatures: (**a**) frontal, (**b**) lateral, (**c**) isometric, and (**d**) isometric.

The lateral view of the dehydrator, highlighting the air-temperature distribution, is seen above. At the bottom, the temperature ranges between 40 and 60 °C, which is ideal for the dehydration process for food. In the mid-section, the temperature generally falls between 60 and 70 °C, with occasional peaks reaching 70 to 80 °C. It is crucial to note that temperatures above 70 °C can cause significant damage to biological products. At the outlet and inlet of the dehydrator, the highest temperatures exceed 100 °C, while the lowest are around 30 °C.

The tray temperatures are also described, and can be observed to range between 43 and 56 °C for the initial three trays, and between 56 and 69 °C for the next four. The temperature of the second tray is maintained between 69 and 82 °C, which represents a significant risk of damage to biological products. Furthermore, the majority of the last tray is heated to 95 °C, indicating that relocating the fan or eliminating the last tray may be necessary to prevent thermal damage in the food being dehydrated. The minimum air velocity in the drying chamber is 0.005 m s^{-1}, while the maximum is 0.97 m s^{-1}. It can be observed that in the majority of the chamber, the velocity is between 0.005 and 0.3 m s^{-1}, which is a bit slower than in Model 1. Efficiency of the heating elements in the equipment is to be desired. One way to achieve it is to take advantage of the principle that hot air is

less dense than cold air and therefore rises. With a vertical flow at the top, this physical phenomenon could be exploited. It may be beneficial to consider the inclusion of a fan in a vertical flow for subsequent models of the dehydrator, in order to assess its performance and determine the potential for better optimization (Figure 6).

A comparative analysis was conducted on the maximum and minimum air temperatures, velocities, and tray temperatures of each version of the equipment. To facilitate comparison, the values of Model 2 were divided by those of Model 1, and the results are shown in Table 1. With regard to the temperature, it can be observed that when the minimum value of the variable is greater than 1.00, the Model 2 dehydrator is at an advantage, as it loses less energy. In regard to tray temperatures, the comparison indicates that Model 1 exhibits superior distribution, which is attributable to its geometric configuration. The last trays near the top of Model 2, therefore, should be eliminated. With regard to the velocity, it can be observed that Model 2 displays a more uniform distribution, which can be verified through a comparison index.

Table 1. Comparison indices of Model 1 and Model 2 for the minimum and maximum of air temperature, tray temperature, and air velocity.

Variable	Model 1	Model 2	Comparison Index
Min. Temperature	30 °C	40 °C	1.33
Max. Temperature	100 °C	100 °C	1.00
Min. Tray Temperature	46 °C	43 °C	0.93
Max. Tray Temperature	70 °C	95 °C	1.36
Minimum Velocity	0.005 m s^{-1}	0.005 m s^{-1}	1.00
Maximum Velocity	1.06 m s^{-1}	0.97 m s^{-1}	0.92

4. Discussion

Dehydration is an important process, due to the fact that it can extend the shelf life of agricultural products and allow the sale of products out of season. This process results in a reduction by one-third in the space requirements for food storage and transportation. With the implementation of renewable energies and intelligent automatic control systems, the energy costs of the process can be reduced [4,5,7,10,23].

In similar studies, it has been recommended that the equipment exhibit a more uniform temperature and velocity distribution within its internal components [5,23]. In the case of Model 2, the drying chamber temperature is distributed uniformly across the surfaces of the trays, with the temperature reaching approximately 60 °C. However, modifications are necessary to enhance the drying process at the top.

Some other designs have a utilized smaller drying chamber. One dryer was reported to be 0.6 m long, 0.35 m wide, and 0.5 m high, with a volume of 0.105 m^3, and with the trays arranged vertically and separated by 0.04 m [5]. Another dryer was designed as low capacity (10–15 kg of product), using six trays. Its drying chamber dimensions are 0.77 m long, 0.65 m wide, and 1.085 m ± 0.125 m high, with a volume of approximately 0.543 m^3 [18]. Another dryer is reported to have a size of 1.25 m length, 0.85 m width, 0.63 m height, and a volume of 0.67 m^3 [11]. A larger equipment configuration is also reported, comprising a drying chamber with a height of 1.4 m, a depth of 0.90 m, a width of 0.5 m, and a volume of 0.63 m^3 [32]. This last chamber is among the largest, yet the Model 2 configuration is three times larger.

The drying chamber of Model 1 has a volume of 2.11 m^3, which is significantly larger than the previously reported designs. The drying volume of Model 2 is 2.02 m^3. The small cabinet-type dryer is well suited to drying small quantities, whereas the multi-shelf dryer is reported as being employed on a larger scale [2]. This approach represents a novel methodology, as it enables the model to be employed for larger-scale production, thereby offering a viable alternative for reducing harvest waste in small greenhouse production.

The solar drying system can be employed in limited crop volumes or on a domestic scale [2]. Solar systems are designed for low-capacity solar drying, yet they are economically

viable for farmers, maintaining product quality [15]. A small solar dryer utilizes the equivalent of 0.12 kW from the sun, and it can heat to 94.8 °C [22].

Unfortunately, Model 1 was unable to achieve an adequate drying temperature. Model 2, however, employs two 2.5 kW heat sources and has proven sufficient for maintaining a 60 °C temperature within the core equipment. Additionally, one advantage of the electrical dryer is that it is not subject to environmental fluctuations and can operate continuously, including during nighttime hours. Although solar drying systems are sustainable, their implementation for commercial-level applications is laborious [5].

Another approach to efficient energy use is the use of hybrid systems, which combine solar and electric energy as heating sources and use automatic control systems. Other studies have reported energy savings between 28–35% without affecting the food quality characteristics of products such as blueberries, raspberries, tomatoes, eggplant, ber fruit, coffee, tobacco, tea, cocoa beans, rice, and nuts [3,5,11,13,15].

Although the proposed Models 1 and 2 are not hybrid systems at this stage, the incorporation of alternative complementation with solar panels for the digital system and solar collectors being used to reduce heat transfer areas is being considered for further versions, with the intention to reduce the energy demand of the designed equipment.

A proper and simple design is fundamental in dryers for an effective utilization of thermal energy. Additionally, the equipment must be able to process differently a huge range of food materials [5]. Model 2 has demonstrated, with the CFD methods, that it will maintain the temperature in a range optimal for the drying processes of agricultural products. Each of these products has a different temperature range for drying, so it is very important that the equipment can adapt to the product selected. A control system that can allow for the selection of the product to be dried and adapt the temperature to that product must be implemented in Model 2. This must be achieved with fuzzy logic, which has been proven to adapt to different circumstances within nonlinear systems [10].

A good mechanical design and a hybrid system of heat sources, combined with a fuzzy logic controller, could result in a more efficient dryer. Additionally, a system larger than the ones previously proposed could make an impact in small-farm production and may help to reduce harvest waste. It is imperative that subsequent models retain these considerations.

5. Conclusions

Simulation is a valuable resource-saving tool that enables the efficient utilization of materials and construction time. In this instance, the CFD methodology enabled the identification of enhancements to the designed dehydrator, with the objective of improving its overall performance.

Two models of dehydrators were designed and evaluated using CFD methods. The initial model was unable to achieve an optimal energy demand. The inlet air required a significant amount of energy to heat the device, and the flow rate was challenging to regulate. These issues were attributed to the model's complex geometry and the positioning of the fan.

The second model had a smaller volume and was lighter in weight, which was achieved through the use of a more efficient geometry. In addition, two fans and two heat sources were considered, resulting in an improved air-temperature distribution. This model is superior, as evidenced by the CFD simulation, and it accomplishes the drying of agricultural products in a temperature range of 40 to 70 °C across a majority of the equipment, making it economically viable for larger production scales than those associated with versions previously reported.

Supplementary Materials: The following supporting information can be downloaded at: https://www.mdpi.com/article/10.3390/app14188472/s1.

Author Contributions: Conceptualization—S.A.R.-R. and G.M.S.-Z.; preparation of the original draft—S.A.R.-R.; reviewing and editing—P.S.F.-A., E.A.R.-A., G.M.-B., and G.M.S.-Z.; supervision—M.T.-A. and G.M.S.-Z. All authors have read and agreed to the published version of the manuscript.

Funding: This research received no external funding.

Institutional Review Board Statement: Not applicable.

Informed Consent Statement: Not applicable.

Data Availability Statement: All data are available in the Supplementary Material.

Acknowledgments: The authors thank the Consejo Nacional de Humanidades Ciencia y Tecnología (CONAHCyT, S.A.R-R 755636) for the scholarships awarded for postgraduate studies.

Conflicts of Interest: The authors declare no conflicts of interest.

References

1. Vega-Mercado, H.; Marcela, M.; Ongora-Nieto, G.; Anovas, G.V.B.-C. Advances in Dehydration of Foods. 2001. Available online: www.elsevier.com/locate/jfoodeng (accessed on 26 July 2024).
2. Sharma, V.K.; Colangelo, A.; Spagna, G.; Trisaia, E.C.R.E. Experimental investigation of different solar dryers suitable for fruit and vegetable drying. *Renew. Energy* **1995**, *6*, 413–424. [CrossRef]
3. Ertekin, C.; Yaldiz, O. Drying of eggplant and selection of a suitable thin layer drying model. *J. Food Eng.* **2004**, *63*, 349–359. [CrossRef]
4. Asnaz, M.S.K.; Dolcek, A.O. Comparative performance study of different types of solar dryers towards sustainable agriculture. *Energy Rep.* **2021**, *7*, 6107–6118. [CrossRef]
5. Mohana, Y.; Mohanapriya, R.; Anukiruthika, T.; Yoha, K.S.; Moses, J.A.; Anandharamakrishnan, C. *Solar Dryers for Food Applications: Concepts, Designs, and Recent Advances*; Elsevier Ltd.: Amsterdam, The Netherlands, 2020. [CrossRef]
6. Esper, A.; Miihlbauer, W. Solar Drying-An Effective Means of Food Preservation. *Renew. Energy* **1998**, *15*, 95–100. [CrossRef]
7. Çiftçioğlu, G.A.; Kadırgan, F.; Kadırgan, M.A.N.; Kaynak, G. Smart agriculture through using cost-effective and high-efficiency solar drying. *Heliyon* **2020**, *6*, e03357. [CrossRef] [PubMed]
8. McCabe, W.L.; Smith, J.C.; Harriot, P. *Operaciones Unitarias*, 7th ed.; McGraw Hill: New York, NY, USA, 2007.
9. Madhankumar, S.; Harish, V.; Jayanth, C.P.; Manikandan, R.; Aswin, N. Automated Moisture Remover for Drying Agricultural Products. In Proceedings of the 2021 7th International Conference on Advanced Computing and Communication Systems, ICACCS 2021, Coimbatore, India, 19–20 March 2021; Institute of Electrical and Electronics Engineers Inc.: Piscataway, NJ, USA, 2021; pp. 1096–1100. [CrossRef]
10. Abdenouri, N.; Zoukit, A.; Salhi, I.; Doubabi, S. Model identification and fuzzy control of the temperature inside an active hybrid solar indirect dryer. *Sol. Energy* **2022**, *231*, 328–342. [CrossRef]
11. Poonia, S.; Singh, A.K.; Jain, D. Design development and performance evaluation of photovoltaic/thermal (PV/T) hybrid solar dryer for drying of ber (*Zizyphus mauritiana*) fruit. *Cogent Eng.* **2018**, *5*, 1507084. [CrossRef]
12. Martynenko, A.; Bück, A. (Eds.) *Intelligent Control in Drying*; CRC Press: Boca Raton, FL, USA, 2019.
13. Jibia, A.U. Microcontroller-based fruit drying system. *J. Sci. Technol. Educ. (JOSTE)* **2015**, *3*, 102–110. Available online: https://www.atbuftejoste.com (accessed on 27 July 2024).
14. Institute of Electrical and Electronics Engineers. *2019 Innovations in Power and Advanced Computing Technologies (i-PACT)*; Institute of Electrical and Electronics Engineers: Piscataway, NJ, USA, 2019.
15. Catorze, C.; Tavares, A.P.; Cardão, P.; Castro, A.; Silva, M.E.; Ferreira, D.W.; Lopes, S.; Brás, I. Study of a solar energy drying system—Energy savings and effect in dried food quality. *Energy Rep.* **2022**, *8*, 392–398. [CrossRef]
16. Ortiz-Rodríguez, N.M.; García-Valladares, O.; Pilatowsky-Figueroa, I.; Menchaca-Valdez, A.C. Solar-LP gas hybrid plant for dehydration of food. *Appl. Therm. Eng.* **2020**, *177*, 115496. [CrossRef]
17. Fabani, M.P.; Román, M.C.; Rodriguez, R.; Mazza, G. Minimization of the adverse environmental effects of discarded onions by avoiding disposal through dehydration and food-use. *J. Environ. Manag.* **2020**, *271*, 110947. [CrossRef] [PubMed]
18. Devi, T.B.; Kalnar, Y.B. Design consideration of smart solar dryer for precision drying. *J. AgriSearch* **2021**, *8*, 135–138. [CrossRef]
19. Jamaleddine, T.J.; Ray, M.B. Application of computational fluid dynamics for simulation of drying processes: A review. *Dry. Technol.* **2010**, *28*, 120–154. [CrossRef]
20. Nielsen, P.V. Fifty years of CFD for room air distribution. *Build. Environ.* **2015**, *91*, 78–90. [CrossRef]
21. Arévalo, J.R.M.; Vargas, E.M.N.; Vásquez, L.F.C.; Mariño, C.J.S. Simulation of a natural thermal insulator application in an indirect solar dehydrator. *Ing. Desarro.* **2021**, *38*, 1–12. [CrossRef]
22. Salisu, S.; Joel, O.O.; Murray, A.O. Design, Construction, and Simulation of a Solar Fish Dryer. *Int. J. Trend Sci. Res. Dev.* **2019**, *3*, 239–244. Available online: https://www.ijtsrd.com (accessed on 26 July 2024). [CrossRef]

23. Castaño-Rodríguez, J.; Amaya, D.; Ramos, O. Food Dryer Design and Analysis of Velocity and Temperature Profiles. *Int. J. Appl. Eng. Res.* **2018**, *13*, 13578–13583. Available online: https://www.ripublication.com/ijaer.htm (accessed on 27 July 2024).
24. Mott, R.L. *Machine Elements in Mechanical Design*, 4th ed.; Pearson Education, Inc.: New York, NY, USA, 2004.
25. Budynas, R.G.; Nisbett, J.K. *Shigley's Mechanical Engineering Design*; McGraw-Hill: New York, NY, USA, 2011.
26. Natarajan, S.K.; Elavarasan, E. A Review on Computational Fluid Dynamics Analysis on Greenhouse Dryer. *IOP Conf. Ser. Earth Environ. Sci.* **2019**, *312*, 012033. [CrossRef]
27. Malekjani, N.; Jafari, S.M. Simulation of food drying processes by Computational Fluid Dynamics (CFD); recent advances and approaches. *Trends Food Sci. Technol.* **2018**, *78*, 206–223. [CrossRef]
28. Oberkampf, W.L.; Trucano, T.G. Verification and validation in computational fluid dynamics. *Prog. Aerosp. Sci.* **2002**, *38*, 209–272. [CrossRef]
29. Dassault Systemes. *Technical Reference Solidworks Flow Simulation 2021*; Dassault Systemes: Waltham, MA, USA, 2020.
30. Arun, K.R.; Srinivas, M.; Saleel, C.A.; Jayaraj, S. Active drying of unripened bananas (Musa Nendra) in a multi-tray mixed-mode solar cabinet dryer with backup energy storage. *Sol. Energy* **2019**, *188*, 1002–1012. [CrossRef]
31. Ouaabou, R.; Nabil, B.; Ouhammou, M.; Idlimam, A.; Lamharrar, A.; Ennahli, S.; Hanine, H.; Mahrouz, M. Impact of solar drying process on drying kinetics, and on bioactive profile of Moroccan sweet cherry. *Renew. Energy* **2020**, *151*, 908–918. [CrossRef]
32. Tagnamas, Z.; Bahammou, Y.; Kouhila, M.; Hilali, S.; Idlimam, A.; Lamharrar, A. Conservation of Moroccan truffle (*Terfezia boudieri*) using solar drying method. *Renew. Energy* **2020**, *146*, 16–24. [CrossRef]

Disclaimer/Publisher's Note: The statements, opinions and data contained in all publications are solely those of the individual author(s) and contributor(s) and not of MDPI and/or the editor(s). MDPI and/or the editor(s) disclaim responsibility for any injury to people or property resulting from any ideas, methods, instructions or products referred to in the content.